

Tunable collective behavior in active cytoskeletal assemblies

Simon L. Freedman, Shiladitya Banerjee, Glen M. Hocky, Aaron R. Dinner

Abstract

Cells can modulate the mechanical properties of the actin cytoskeleton in remarkable ways to maintain structural integrity, move and divide. This behavior is achieved through crosslinking proteins and bundling agents that dynamically control cellular structure, as well as active motors that generate active stresses and regulate intracellular transport. *In vitro* model systems using a small subset of purified proteins have revealed the minimal components necessary to confer this wide range of mechanical behaviors. Here, we take the same approach using agent-based computational modeling, and investigate the collective dynamics of disordered cytoskeletal assemblies, consisting of semi-flexible filaments, dynamic crosslinkers, and molecular motors. By tuning the properties of individual cytoskeletal elements, such as filament length, crosslinker stiffness, or motor kinetics, we explore the collective phases of actomyosin networks across dynamic regimes inaccessible to experiments. Our work elucidates the diverse pathways for cytoskeletal contractility, polarity organization, and molecular transport, and provides testable predictions for future experiments on reconstituted cytoskeletal assemblies.

1 Introduction

The actin cytoskeleton serves as a dynamic scaffold that allows eukaryotic cells to actively change shape, move, and adapt to their micro-environment. Although the cellular cytoskeleton constitutes a complex network of protein-protein interactions, *in vitro* model systems have revealed the minimal set of components required to exhibit a wide range of active mechanical behaviors including contractility and polarity organization [1–3]. In this work, we investigate the range of collective behaviors accessible to a minimal system consisting of cytoskeletal filaments, crosslinking proteins, and active molecular motors. While previous studies have shed light on the mechanisms of contractility and self-organization in minimal cytoskeletal systems [1, 3–7], a necessary limitation is the difficulty to precisely control physical properties of their protein constituents. Thus, it is poorly understood how variations in filament stiffness, length, crosslinker geometry, and affinity control emergent properties of cytoskeletal assemblies. Here, we present an agent-based model of the actin cytoskeleton, using non-equilibrium molecular dynamics, that can efficiently explore the collective phases of crosslinked actomyosin networks. Our agent-based model is ideal for elucidating the relationship between protein-protein interactions at the microscale and the collective mechanical behavior of the assembly. Furthermore, our dynamic simulations enable us to learn how active networks sample through dynamic states, and how intermediate mesoscopic structures may tune network functionality at cellular scales.

Actomyosin contractility has been extensively studied in the context of muscle cells, where actin filaments are arranged in a sarcomeric fashion, enabling myosin minifilaments to translocate two anti-parallel actin filaments and yield active muscle contraction [8]. However, the cytoskeleton of nonmuscle cells, exhibits no inherent ordering of actin or myosin filaments, yet F-actin buckling has been shown to coordinate long-range contractile behavior [1, 9, 10]. Recent *in vitro* studies using reconstituted networks of actin and myosin, have revealed how changing myosin concentration and F-actin properties effect the ability of a disordered networks to contract and form static structures [1, 2, 11]. For instance, at low motor density, the actin network behaves as non contractile, resulting in long-distance translocation of myosin along actin tracks [12]. Above a critical density, myosin motors cooperatively contract the actin network. Additionally, it has been shown that actin binding proteins (crosslinkers) such as filamin, scruin, and α -actinin, can profoundly affect long-range force propagation as well as the mechanical stability of actin bundles and network [1, 2, 10, 13]. While these experiments are beginning to suggest the phase space of collective behavior in active networks, agent based simulations can explore in a controlled fashion how myosin density, actin bundle rigidity, and crosslinker density are able to modulate structure formation and force generation within the cell cytoskeleton.

To probe the microscopic origin of these complex collective processes, we propose an agent-based simulation model, motivated both by *in vitro* experiments as well as *in vivo* mechanical studies on actin and myosin [14, 15]. Our model also incorporates essential features from previous modeling work. Some of these models were designed to understand rheological properties of crosslinked actin networks [16–19], some have investigated the collective motion of motors on cytoskeletal tracks [20–22], and others have shown how disordered assemblies of filaments and motors collectively form asters [23] or induce network-level contraction [5–7, 24]. We use the worm-like chain model for an actin filament with both bending and stretching energies [20] and initialize networks with crosslinkers at filament intersections to form well connected networks [17]. In contrast to references [5, 17], we simulate non-equilibrium dynamics, including thermal fluctuations, stochastic binding and unbinding kinetics of myosins and crosslinkers, and myosin translocation. Force propagation rules, binding kinetic equations, and motor precession will be similar to [20, 23] with minor differences in implementation.

We accurately bench-mark our simulations to reproduce well known experimental results for actin filament dynamics, as well as the collective behavior of crosslinked actin and myosin driven active networks. We quantitatively reproduce the experimentally measured spatio-temporal fluctuations of single actin filaments. For passive crosslinked networks we recover the well-established stress strain relationships measured for semiflexible polymer networks [13, 25–27]. For active networks, we reproduce the experimentally observed velocity distributions of actin filaments in an actomyosin motility assay. These results demonstrate that our simulations capture several key properties of cytoskeletal networks within a single agent-based model.

We then show that our simulations predict diverse collective dynamical behaviors in cytoskeletal assemblies, and that tuning properties of filaments, crosslinkers, and motors, effects this collective behavior. We find that crosslinker affinity modulates filament bundling and network coarsening in a biphasic manner. We further show that crosslinker stiffness can tune the strain stiffening response of actin networks in a simulated rheology experiment. We quantify motor-dependent contraction in active networks and predict how the concentration of motors controls actin polarity sorting. These results suggest actomyosin contractility emerges from a competition between bundling and polarity sorting. We characterize study how variations in actin filament length, motor density, and motor-filament binding can alter motor cooperativity to translocate actin filaments, which may have implications for optimizing the observed dy-

namics of polarity sorting and contractility. Collectively our work demonstrates how ensembles of randomly oriented actin filaments and crosslinkers can be rearranged by myosin motors to form tunable structures with distinct biophysical and mechanical functionalities.

2 Results

An essential mechanical function of actomyosin networks is their contractility, which coordinates a variety of cellular processes, including muscle contraction, cell motility and division. That these complex macroscopic mechanisms arise stochastically from simple microscopic interactions suggests the ability to engineer materials with controllable network topologies and dynamics. Recently, in-vitro experiments of reconstituted actomyosin networks have demonstrated this controllable architecture by varying motor density and crosslinker density and showing how they effect contractility [1, 2]. Our model shows a similar dependence of network contractility on motor density. Additionally, we demonstrate tunability between two modes of network organization: bundling, in which dynamic crosslinkers align filaments into robust networks, and polarity sorting, in which motors organize filaments into structures of uniform polarity.

For computational efficiency we have chosen to coarse grain actin filaments and crosslinker proteins at length scales relevant for network behavior. Actin filaments are modeled as polar worm-like chains (WLC) such that one end of the chain represents the barbed end of a filament and the other end represents its pointed end. Crosslinkers are modeled as Hookean springs such that both ends of the spring (heads) can bind and unbind from filaments. A schematic of these network components is shown in Figure 1B, while the load dependent kinetics of crosslinkers, and the force-extension relationships for both filaments and crosslinkers are shown in Figure 1C.

Experiments have shown that adding crosslinkers to assemblies of F-actin yields actin bundles [1, 2, 13] and that increasing crosslinker density can increase the length scale of contraction [1]. We show that varying the stiffness of these springs modulates the rheology of an assembly of crosslinkers and filaments, while varying the binding affinity effects the magnitude of actin bundling. We parameterized our model in 2D similar to the nearly flat in vitro reconstitutions of actomyosin. This setup is sufficient to reproduce structures of biological interest, and allows us to simulate large systems for long times. Because we use a 2D system to model a 3D experiment, we exclude the steric interactions of filaments and crosslinkers, to allow for some of the freedom lost from the reduction in dimensionality.

2.1 Crosslinker turnover modulates bundling of filament networks

The rapid binding and unbinding of crosslinking proteins from actin filaments can reorganize initially disordered filament networks into thick bundled networks. This behavior is distinct from motor-driven contractility, because the overall network structure coarsens without any active force generation. Here we tune this bundling mechanism by changing the crosslinker-filament binding affinity.

To demonstrate this behavior, thirteen simulations were initialized with 500 $15\mu\text{m}$ worm-like-chain filaments scattered on a $(75\mu\text{m})^2$ simulation cell, and $0.15\mu\text{m}$ crosslinkers placed at filament-filament intersections as shown in Figure 1A. The assemblies were evolved via Brownian dynamics for 200s. Each simulation had a different dissociation rate for crosslinkers k_{off}^{cl} varying logarithmically between $0 - 1800\text{s}^{-1}$. The results, shown in Figure 2A, indicate

that for certain initializations the crosslinkers bundled actin filaments to yield highly connected networks.

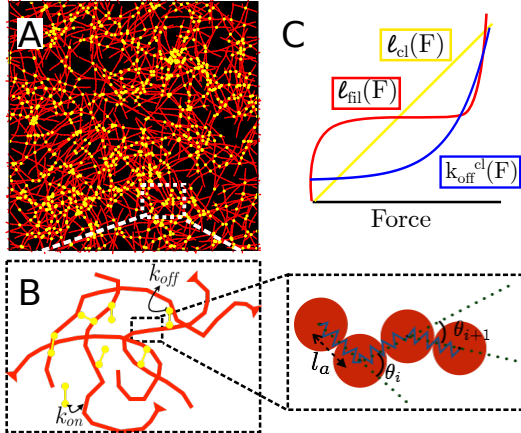


Figure 1: Computational actomyosin network representation. (A) Initial configuration of an assembly of actin filaments (red) which initially have crosslinkers (yellow, one third shown) placed at intersections. Cell size is $(75\mu\text{m})^2$. (B) Zoom in of the network revealing that crosslinkers can attach and detach to actin filaments, as well as the bead-spring filament representation of actin described in Methods. (C) Schematic of the load dependent detachment rate of crosslinkers, the linear stiffness of crosslinkers, and the nonlinear force extension curve for filaments.

We have quantified the structural rearrangements inherent in bundling by the emergent density heterogeneity and local alignment. Density heterogeneity, is measured using the radial distribution function of actin filaments $g(r) = P(r)/(2\pi r \delta r \rho)$ where $P(r)$ is the probability that two beads on different filaments are separated by a distance r , $\delta r = 0.05\mu\text{m}$ is the bin size and $\rho = 500/(75\mu\text{m})^2$ is the number density. Figure 2B shows that for the a bundled configuration the width of the peak of $g(r)$ increases over time indicating that more actin filaments are brought closer together. Local alignment of actin filaments is measured via the 2D nematic order parameter $s_2 = 2\langle \cos^2 \phi_i \rangle - 1$, where ϕ_i is the angle between a filament link and its local director, defined as the average angle of links less than a distance of $1\mu\text{m}$.

Figure 2C shows that $g(r)$ for the final configuration ($t = 200s$) shows a non-monotonic dependence on crosslinker detachment rate. Similarly, Figure 2D, shows that over time, the nematic order of these more bundled networks increases to a higher value than the lower bundled networks. Together, Figure 2C-D indicate that a low disassociation rate does not allow for significant restructuring from the initially random configuration, and a high disassociation rate will not yield long-lived stable structures. However, at intermediate values of k_{off}^{cl} , the filaments self-assemble into a stable, thickly bundled network. This relationship is in contrast to the dependence of bundling on crosslinker density, which as shown in the Supplement indicates that more crosslinkers yield more bundling.

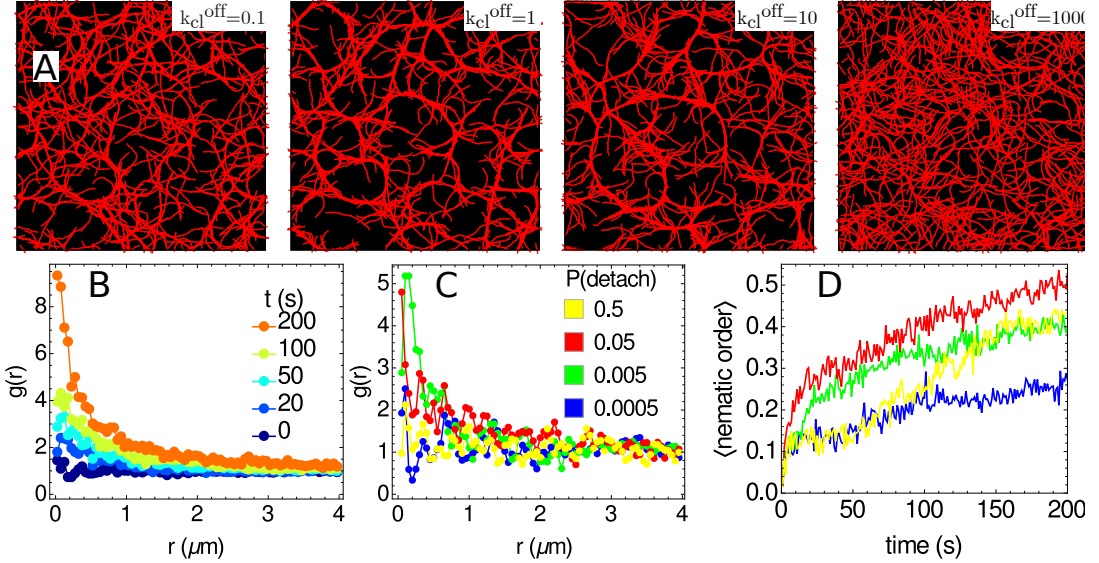


Figure 2: Dependence of network bundling on crosslinker detachment rate. (A) Network configuration at $t = 200$ s for varying disassociation constants of crosslinks (not shown). Filaments are shown in red. (B) Radial distribution function of beads on an actin filament for the $k_{off} = 20 \text{ s}^{-1}$ at various times throughout the simulation. (C) Radial distribution function of actin filaments at $t = 200$ s for varying k_{cl}^{off} . (D) Local ematic order of actin filaments as a function of time for the same values of k_{cl}^{off} .

2.2 Cooperative sorting of filament polarity by molecular motors

Molecular motors are modeled as active crosslinkers such that a bound head precessively walks toward the barbed end of the filament with load dependent speed and kinetic (see Methods for details). This implementation allows for active filament sliding and filament buckling, as elucidated in Figure 3, both of which are instrumental for actomyosin contractility [1]. In large networks, motors can translocate across filaments, induce filament buckling, and also enhance network connectivity [2].

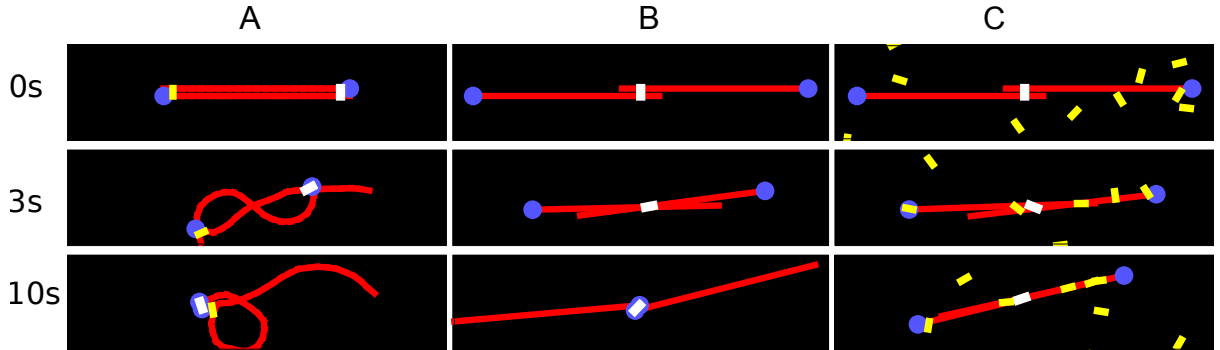


Figure 3: Time series of three antiparallel $10 \mu\text{m}$ filaments (red) interacting with a minimal set of motors (white) and crosslinkers (yellow) for 10s . Barbed ends of filaments are marked by a blue dot. (A) Filaments are semiflexible (21 bead-spring chain) and pinned on the left by a crosslinker, so the motor-filament interaction yields contraction via buckling. (B) Filaments are rigid (2-bead-spring chains) and unpinned, so motor-filament interaction yields unimpeded sliding of filaments. As a result, they transition from an initially extended state, to a contracted state at $t = 3\text{s}$ and back to a fully extended polarity sorted state at $t = 10\text{s}$. (C) Filaments and motor are the same as (B) but with a population of crosslinkers near the filaments that arrests the filaments in a contracted state.

To isolate the role of active motors on assemblies of semiflexible filaments, the actin assembly in Figure 1 was generated without crosslinkers at filament intersections, but with $0.5\mu\text{m}$ long motor minifilaments scattered uniformly throughout the simulation cell. In these simulations, the motor duty ratio was kept near unity to replicate the behavior of a myosin minifilament, while the density of motors was varied between different simulations. The results, shown in Figure 4, indicate that at higher motor densities, filaments are sorted by polarity, but are not clustered in space. Motors aggregated on the barbed ends of filaments and thereby brought the different barbed ends together to form asters. The magnitude of polarity sorting was measured by calculating the contribution to the radial distribution function by the barbed ends of actin filaments. This value, $g(r_{barb})$ is shown in Figure 4B and peaks at significantly higher values than $g(r)$. It is clear from this figure that the degree of polarity sorting is highly dependent on motor density.

A secondary peak is visible in Figure 4 at $r_{barb} \approx 0.5\mu\text{m}$, which is the rest length of the molecular motors. This indicates that the motors responsible for polarity sorting remain at the center of asters. We calculate the average distance of a bound motor from the barbed end of filament to which it was bound to verify that this is the mechanism of polarity sorting. As seen from Figure 4C-D, increasing motor density had the effect of decreasing this distance, indicating a larger magnitude of polarity sorting. Thus, motor density tunes the magnitude of polarity sorting in assemblies of motors and filaments. Motor-filament affinity also plays an important role (see Supplement) where we have shown that the most polarity sorted networks emerge from intermediate values of motor detachment.

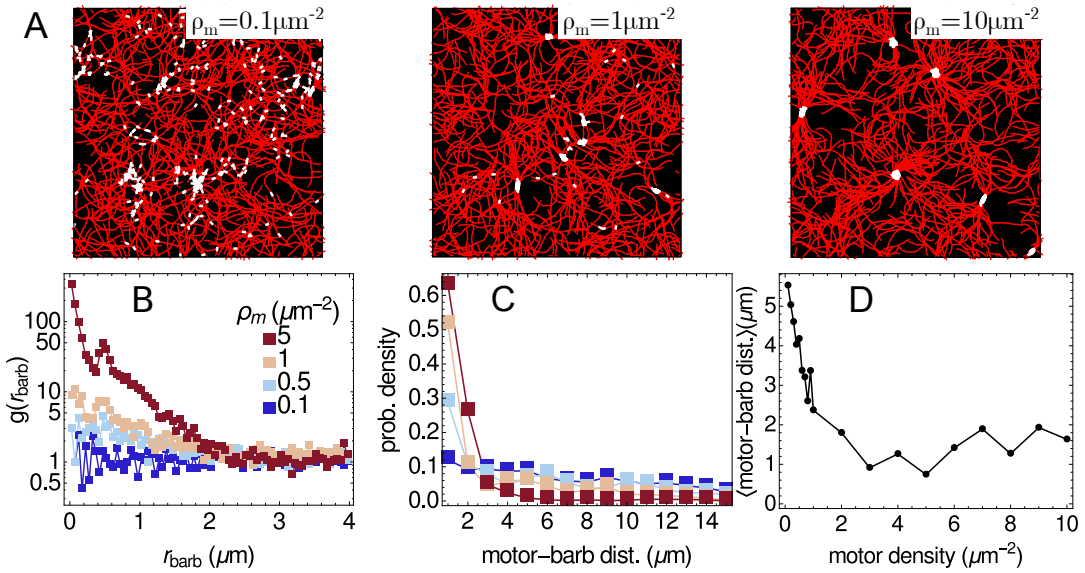


Figure 4: (A) Networks at their polarity sorted end configuration ($t = 96\text{s}$). Filaments are shown in red, motors in white. A maximum of 1000 motors are shown in each case. (B) Radial distribution function for barbed ends ($t = 96\text{s}$) shows a strong dependence on motor density. For $\rho_m = 5\mu\text{m}^{-2}$, a prominent secondary peak is also visible at the motor rest length $l_m = 0.5\mu\text{m}$. (C) Probability density of the distance of an attached motor head from the barbed end of the filament to which it is attached for the same simulations. (D) The average distance of a motor head from the barbed end as a function of motor density.

2.3 Contractility emerges from competition between bundling and polarity sorting

When both crosslinkers and motors are mixed with semiflexible filaments, the assemblies become contractile. To elucidate this behavior, actin filament assemblies were initialized (see Figure 1) with crosslinkers at their intersections with motors scattered uniformly throughout the cell. The motor density varied between simulations from $0.1 - 10 \mu\text{m}^{-2}$. The crosslinkers were kept sticky with a low duty ratio, while the motors were highly active with a high duty ratio. This ensured that connectivity of the network was almost exclusively controlled by crosslinkers while force generation was controlled by motors.

The results of these simulations and the final network configurations can be seen in Figure 5. The net contractility was measured by interpolating a velocity field from the displacement vectors of filament beads from each simulation snapshot, measuring the divergence at each point on the vector field, and summing the values. A negative total divergence of a given snapshot indicates at that time the network was contractile. As evident in Figure 5B higher motor density leads to larger contractility. Figure 5C-D shows that actin buckling, here measured as the change in the end to end distance Δs of an actin filament:

$$\Delta s = \left(1 - \frac{|r_{15} - r_0|}{\sum_{i=1}^{15} |r_i - r_{i-1}|} \right) \quad (1)$$

correlates with contractility, suggesting that the primary mechanism driving contractility in these flexible networks is filament buckling, as observed in experiment [1]. Networks with low motor densities and extremely low motor disassociation rates (both with and without crosslinkers) were also shown to be contractile, as seen in the supplement.

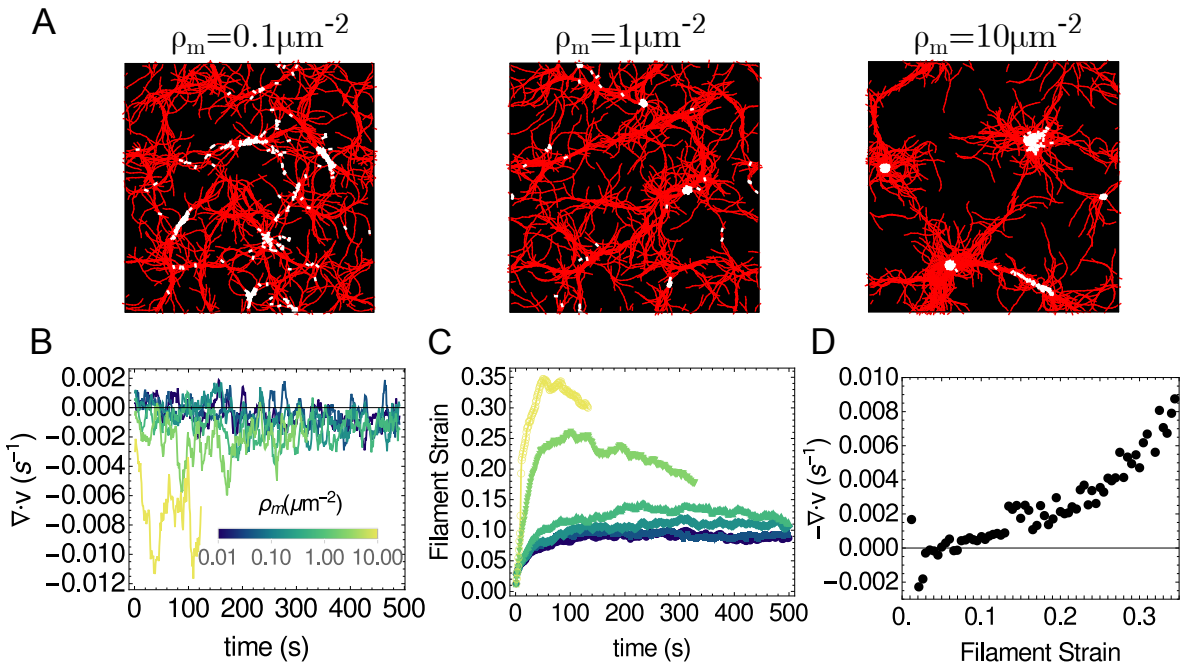


Figure 5: Assemblies with motors and crosslinkers yield contraction. (A) Networks configurations at their largest contractile strains for different motor densities. Filaments are shown in red, and motors in white. Only 1000 motors are shown in each case. (B) Spatially averaged divergence of filament flow field as a function of time for networks of varying motor density. (C) Average filament strain (defined in Equation (1)) as a function of time for the same networks. (D) Correlation between filament strain and the network strain averaged over bins of size 0.005 for all motor densities

3 Discussion

The goal of this paper is to introduce a framework that could accurately and efficiently simulate active networks of filaments, motors, and crosslinker proteins and predict the various structural and mechanical phases of the system. We have successfully shown that crosslinkers can bundle filaments into thick, connected networks, motors can sort filaments into structures of homogenous polarity, and both can work together to yield actomyosin contraction. We have characterized the bundled networks via their local alignment, polarity sorted networks by the radial distribution function of filament barbed ends, and demonstrated contractility by measuring instantaneous network divergence. We summarize these results in Figure 6.

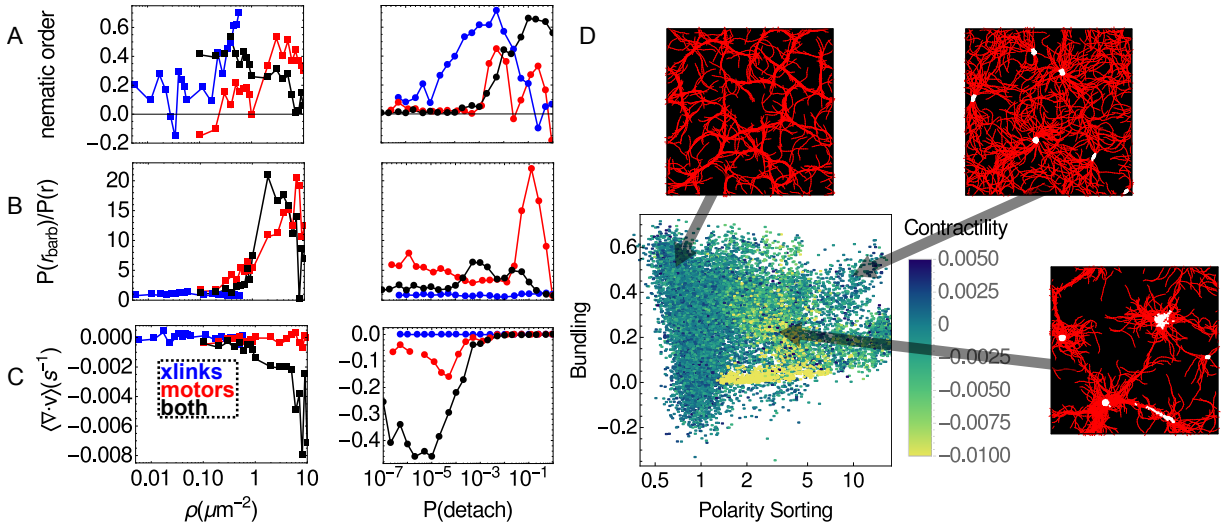


Figure 6: Structural phases of crosslinked actomyosin networks. For blue data points, ρ and $P(\text{detach})$ parameterizes the crosslinkers, while for red and black curves, they parameterize the motors. (A) Nematic order of structures emergent from a range of densities and rates for motors and crosslinkers. (B) The probability that filament barbed ends are separated by less than $1\mu\text{m}$ with respect to the probability that arbitrary filament positions are separated by less than $1\mu\text{m}$. (C) Total divergence of these networks. Extremely low values at low detachment rates indicate that the network was ripped apart. (D) Phase diagram of all networks at all times. Bundling is measured via nematic order, polarity sorting as $P(r_{\text{barb}})/P(r)$ and contractility as total divergence.

Figure 6A shows that we have characterized bundling using the nematic order parameter and that the most locally aligned networks occur when only crosslinkers are present. This alignment can be tuned by varying both crosslinker density and crosslinker detachment rate. For networks with both motors and crosslinkers, bundling occurs when motors have a high detachment rate, as the polarity sorting mechanism is dominated by the bundling mechanism. In Figure 6B, we have measured polarity sorting by calculating the probability that two filament barbed ends are separated by a distance of less than $1\mu\text{m}$ with respect to the probability that arbitrary positions on a filament are separated by a distance of less than $1\mu\text{m}$. In this case motors are the key restructuring agent, and higher motor density yields a stronger polarity sorting effect. The introduction of a small population of crosslinkers inhibits this effect slightly, as seen from the black curve in the left hand plot of Figure 6B, and contraction begins to dominate. Network contraction dependence on density and detachment rates is measured via the total divergence (summed over space and time) shown in Figure 6C, where it is clear that the combination of motors and crosslinkers yields the highest values of contraction and that one can tune this effect by varying motor density and motor detachment rate. We used these order parameters to

develop a phase diagram (Figure 6D) and show that bundling, and polarity sorting, are distinct structural phases which can couple to yield contractile behavior.

Each of these structural organization techniques have distinct *in vivo* biomechanical applications. Actin bundles can function as force chains to propagate stress large distances across the cell, and bundled networks can be used to stabilize the cell interface, which may be necessary for the formation of an immunological synapse [28]. Polarity sorting can yield directed networks useful for long distance transport of material across the cell. Actomyosin contraction is necessary for diverse cell-morphology phenomena including motility and division.

Other actomyosin models have explored the driving mechanisms behind contractility and structure formation. Dasanyake, et. al., extended the equilibrium, 2D crosslinked rigid filament network model in [17] to include a term in the potential energy that corresponded to myosin motor activity, and observed the emergence of force chains that transmit stress throughout the network [5]. Wang and Wolynes [6] model the F-actin networks as a graph of crosslinkers (nodes) and rigid actin filaments (edges) in which myosin motor activity is simulated via antisymmetric kicks along the filaments and predict a binary phase diagram of networks which are either contractile or not as a function of cross linker and myosin densities. While the simplicity of these models is intriguing, they do not account for explicit filament buckling, and their integration is performed via Monte Carlo, more applicable to structure formation than dynamics. Nedelec used dynamic simulations of ensembles of filaments and motor proteins to explore aster formation in microtubule-kinesin assemblies, as well as motility and contractility in actomyosin [4, 7, 20]. Kim used an agent based approach of filaments, motors and crosslinkers, to explore a variety of topics, including bundling via parallel actin crosslinkers and force generation by myosin motors [24, 29]. As seen in Methods, we have benefited from the computational techniques explored in each of these theoretical models. We have contributed to this area by showing that a single model can capture many relevant biophysical structures, precisely quantifying these behaviors and showing how to tune them via experimentally manipulatable physical parameters.

While our model is thorough in what it aims to simulate it is limited by a few experimental observations that are currently not implemented. First, the structure of myosin minifilaments is significantly more complex than a two headed spring. As mentioned, these minifilaments have dozens of heads, which allows them to walk along multiple filaments and could result in subdiffusive behavior [30] and significantly increase local network elasticity [31]. Another limitation of our system is that the actin filaments are static, and will not polymerize, depolymerize or sever. Within actomyosin assays it is clear that recycling of actin monomers and to a lesser degree, filament severing plays an important role in contraction [1]. Within the cytoskeleton, actin treadmilling is also important for shape production. Additionally, these simulations are all run in 2D and without steric interactions, and dimensionality and volume exclusion may play important roles. While we intend to address and investigate these limitations in future works, we believe that the successful benchmarking of the simulation at various levels is a significant argument in favor of the current setup.

There are still many unanswered questions regarding self-organization in actomyosin networks that we hope can be addressed using this simulation, such as how actomyosin controls the shape of cell membranes, and how they form force propagating chains across the cytoskeleton [5, 32]. In particular, it is significantly easier to measure internal active forces and energies in simulation than in experiment, so we expect this model will aid the process of isolating the particular mechanisms involved in restructuring these polymer assemblies. We stress, however, that the applicability of such a simulation package reaches beyond studying the phases of actomyosin networks. We believe this simulation can shed light on the mechanics and dynamics of

a variety of active polymer assemblies.

Similar networks that involve other proteins also exist in the cytoskeleton, such as microtubule-kinesin-dynein networks and could be investigated using this simulation methodology. Furthermore, the cytoskeleton demonstrates how populations of simple machines can self assemble into active materials with useful mechanical properties, and one can use this simulation to efficiently design these types of self assembled materials. Thus, the non-equilibrium molecular dynamics framework of this simulation can be used to model and study many open questions in active matter and biophysics.

4 Methods

4.1 Actin Filaments

Actin filaments are treated as a worm-like chain, with each filament represented as a set of $N + 1$ beads connected by N harmonic springs (links), with an additional harmonic angular potential applied on the $N - 1$ angles along the chain, as depicted in Figure 1B. The linear springs penalize stretching of individual subunits and the $N - 1$ angular harmonic springs penalize bending and enforce the length scale over which the filaments are semi-flexible. The internal forces on actin filaments can be obtained from the gradient of the potential energy U_f

$$U_f = U_{stretch} + U_{bend} \quad (2)$$

$$U_{stretch} = \frac{k_a}{2} \sum_{i=1}^N (|d_i| - l_a)^2 \quad (3)$$

$$U_{bend} = \frac{\kappa_B}{2l_a} \sum_{i=2}^N \theta_i^2$$

where $d_i = r_i - r_{i-1}$, $\theta_i = \arccos\left(\frac{d_i \cdot d_{i-1}}{|d_i||d_{i-1}|}\right)$, k_a is the stretching force constant, κ_B is the bending modulus, and l_a is the equilibrium length of a link.

The value for κ_B was chosen based on the persistence length of F-actin, $L_p \approx 20\mu m$, since $\kappa_B = L_p * k_B T$ where T is the temperature and k_B is Boltzmann's constant [33]. We verified that the measured persistence length of the model filaments agreed with our input bending modulus as seen in Figure 7A. A second (Figure 7B) test was performed to verify that the temporal fluctuations of our filaments corresponded to theoretical predictions for semiflexible filaments [34]. Details of these measurements, as well as explanations for the parameter value choices for l_a , and k_a are available in the supplement.

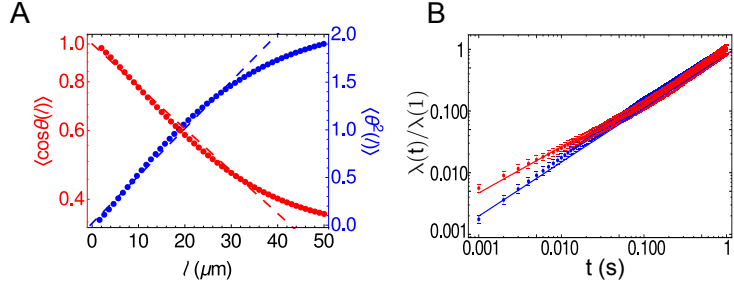


Figure 7: Correlations of actin filaments in space and time. (A) Decorrelation of tangent vectors (red dots) and fluctuations in angles between links (blue dots) as a function of the arc length between them. Red dashed line is $e^{-s/2L_p}$ shows the expected behavior from the input bending modulus of $0.08pN - \mu m^2$ and blue dashed line has slope $1/L_p$. (B) Eigenvalues of covariance matrices for the positions of endpoints of filaments as a function of time. Blue dots shows the longitudinal fluctuations and the red dots shows the transverse fluctuations. Red dashed line is $t^{3/4}$ and blue dashed line is $t^{7/8}$ as predicted by [34].

4.2 Crosslinkers

Crosslinker proteins dynamically connect actin filaments, thereby propagating force from one to another. Thus model crosslinkers, must be able to attach and detach from actin filaments, and be compliant in order to propagate force. They are therefore modeled as hookean springs, with stiffness k_{cl} and rest length l_{cl} . Like actin filaments, the Young's modulus of most crosslinkers is significantly higher than would be reasonable to simulate; therefore we set $k_{cl} = 1-100pN/\mu m$ was so that the bending mode of actin filaments was significantly softer than the stretching mode of crosslinkers. Their rest length l_{cl} differs by the type of cross-linker and ranges from $10nm$ for fascin to $150nm$ for filamin.

At each time step of the simulation an unattached crosslinker head is allowed to attach to nearby filaments and an attached crosslinker head can detach. The probability of a head attaching to an actin filament is a Gaussian distributed random variable, such that

$$P_{cl}^{on} = k_{cl}^{on} dt \exp(-r^2/R^2) \quad (4)$$

where r is the shortest distance from the head to the actin filament and $R = \sqrt{\frac{2k_B T}{k_{cl}}}$ where k_B is Boltzmann's constant and T is the temperature. For crosslinker detachment we model the behavior as that of a slip bond, such that a higher tensile force along the crosslinker backbone will result in a higher probability of detachment [35]. Thus,

$$P_{cl}^{off} = k_{cl}^{off} dt \exp(Fx_{cl}/k_B T) \quad (5)$$

where F is the force along the crosslinker backbone, and x_{cl} is a characteristic bond length [22].

When a crosslinker is bound to a filaments at both ends, it will necessarily be stretched or compressed. If it were allowed to relax independently of the actin filaments to which it is bound it would no longer lie on those filaments. Therefore, the tensile force stored on a stretched or compressed crosslinker is propagated onto those actin filaments via the lever rule outlined in [4, 23]. Thus, if the tensile force of a motor at point r_j between filament beads i and $i + 1$ is F_{cl} , then,

$$\begin{aligned} F_i &= F_{cl} \left| \left(\frac{r_j - r_i}{r_{i+1} - r_i} \right) \right| \\ F_{i+1} &= F - F_i \end{aligned} \quad (6)$$

will be the forces on beads i and $i + 1$ respectively due to the crosslinker.

4.3 Motors

Within the cytoskeleton, tens of myosin II motors aggregate into bipolar ensembles called myosin minifilaments [22]. Since myosin also functions to increase the local elasticity of networks wherever it is bound, the myosin is modeled similarly to a crosslinker, with the subscript m replacing the subscript cl in Equations (4) and (5) and section 4.2 One extra parameter is needed k_m^{end} for the detachment of myosin from the barbed end of a filament, as detachment from the end occurs at different rates than from the rest of the filament.

Unlike crosslinkers, motors process towards the barbed end of actin filaments to which they are bound at speeds that vary depending on the tensile force along the crosslinker [22]. While the mechanochemical process through which individual myosin molecules walk along actin filaments is complex, motility assay experiments have shown that on average bound myosin II walk at an unloaded speed of $v_0 \approx 1\mu m/s$ along actin filaments [36]. A mean field approximation would therefore yield that minifilaments would also precess toward filament barbed ends at $1\mu m/s$ (although see [22] and [37] for higher order measurements). Therefore the relationship between motor velocity and tensile force is modeled linearly, such that the motor head will speed up if the minifilament is compressed (pre-powerstroke) and slow down if the minifilament is stretched (post powerstroke) going to 0 when the force on the minifilament is the stall force $F_s \approx 3.85pN$ [4, 23]; i.e.,

$$v(F_{||}) = v_0 \left(1 - \frac{F_{||}}{F_s}\right) \quad (7)$$

where $F_{||}$ is the force on the motor, projected along the tangent vector of the actin filaments. The minor differences between crosslinkers and motors allow us treat them equivalently, by setting $v_0 = 0$ for the crosslinkers.

4.4 Dynamics and Environment

We solve for the motion of actin filaments using Brownian dynamics (see Supplement for justification), so that at each time, the position of each filament bead and motor (crosslinker) head is updated via the equation

$$r(t + \Delta t) = r(t) + F(t)\mu\Delta t + B(t)\mu\Delta t \quad (8)$$

where $F(t)$ is the sum of internal and external forces on the bead (head), and $\mu = (4\pi R\nu)^{-1}$ where ν is the environment's dynamics viscosity. For the Brownian term, we use the form of Leimkuhler and Matthews [38, 39] that has been shown to minimize deviations from canonical averages in harmonic systems,

$$B(t) = \sqrt{\frac{2k_B T}{\mu\Delta t}} \left(\frac{W(t) + W(t - \Delta t)}{2} \right) \quad (9)$$

where $W(t)$ is a Wiener process, in this case a random number drawn from the normal distribution with mean zero and standard deviation of unity.

We use periodic boundary conditions so as to limit effects of a boundary and to mimic a system larger than the one we simulate. The value for Δt in Equation (8) generally depends on both the unloaded myosin speed v_0 and the largest stiffness in the simulation k_f . For $k_f = 1pN/\mu m$ and $v_0 = 1\mu m/s$ a value of $\Delta t = 0.0001s$ was sufficiently low to solve Equation (8) for hundreds of seconds without spuriously generating configurations of very large energy. The length

and width of the simulations were chosen so as to be high enough to avoid boundary artifacts. Pseudocode of the complete simulation and a description of the neighbor list implementation, used to calculate motor (crosslinker) binding, is available in the supplement. A complete list of simulation parameters used throughout this article is provided in Table 1.

5 Acknowledgements

We thank M. Gardel, J. Weare, C. Matthews, F. Nedelec, F. Mackintosh, and M. Murrell for helpful conversations. This research was supported in part by the University of Chicago Materials Research Science and Engineering Center (NSF Grant No. 1420709). S.L.F. was supported by the DoD through the NDSEG Program. G.M.H. was supported by an NIH Ruth L. Kirschstein NRSA award (1F32GM113415-01).

References

- [1] Michael P. Murrell and Margaret L. Gardel. F-actin buckling coordinates contractility and severing in a biomimetic actomyosin cortex. *Proceedings of the National Academy of Sciences*, 109(51):20820–20825, 2012.
- [2] Michael Murrell and Margaret L. Gardel. Actomyosin sliding is attenuated in contractile biomimetic cortices. *Molecular Biology of the Cell*, 25(12):1845–1853, 2014.
- [3] Kingo Takiguchi. Heavy meromyosin induces sliding movements between antiparallel actin filaments. *Journal of biochemistry*, 109(4):520–527, 1991.
- [4] François Nédélec. Computer simulations reveal motor properties generating stable antiparallel microtubule interactions. *The Journal of Cell Biology*, 158(6):1005–1015, 2002.
- [5] Nilushi L. Dasanayake, Paul J. Michalski, and Anders E. Carlsson. General mechanism of actomyosin contractility. *Physical Review Letters*, 107(11):118101, 2011.
- [6] Shenshen Wang and Peter G. Wolynes. Active contractility in actomyosin networks. *Proceedings of the National Academy of Sciences*, 109(17):6446–6451, 2012.
- [7] Hajar Ennoumani, Gaëlle Letort, Christophe Guérin, Jean-Louis Martiel, Wenxiang Cao, François Nédélec, M Enrique, Manuel Théry, and Laurent Blanchoin. Architecture and connectivity govern actin network contractility. *Current Biology*, 26(5):616–626, 2016.
- [8] H.E. Huxley. The mechanism of muscular contraction. *Science*, 164(3886):1356–1366, 1969.
- [9] Martin Lenz, Todd Thoresen, Margaret L Gardel, and Aaron R Dinner. Contractile units in disordered actomyosin bundles arise from f-actin buckling. *Physical review letters*, 108(23):238107, 2012.
- [10] Michael Murrell, Patrick W. Oakes, Martin Lenz, and Margaret L. Gardel. Forcing cells into shape: the mechanics of actomyosin contractility. *Nature Reviews Molecular Cell Biology*, 16(8):486–498, 2015.

Table 1: Parameter Values

| Symbol | Description (units) [ref] | L_p | Shear | Motility Assay | Networks |
|-----------------------------|--|-----------|--------------------|----------------------|----------------------|
| Actin Filaments | | | | | |
| N_B | Number of beads | 21 – 201 | 16 | 16 | 16 |
| l_a | Link Rest Length (μm) [40] | 1 | 1 | 1 | 1 |
| k_a | Stretching Force Constant ($pN/\mu m$) | 0.01 – 10 | 10 | 1 | 1 |
| κ_B | Bending Modulus ($pN\mu m^2$) [41] | 0.002 – 5 | 0.08 | 0.08 | 0.08 |
| Myosin Minifilaments | | | | | |
| l_m | Rest Length (μm) [42] | n/a | n/a | 0.5 | 0.5 |
| k_m | Stiffness ($pN/\mu m$) | n/a | n/a | 1 | 1 |
| k_m^{on} | Attachment rate at distance $r = 0$ (s^{-1}) | n/a | n/a | 2 – 4000 | 3600 |
| k_m^{off} | Unloaded head detachment rate (s^{-1}) | n/a | n/a | 200 | 200 |
| k_m^{end} | Unloaded head detachment rate at the barbed end of the filament (s^{-1}) | n/a | n/a | 2000 | 2000 |
| x_m | characteristic bond length (μm) [22] | n/a | n/a | 0.0004 | 0.0004 |
| v_0 | Unloaded speed ($\mu m/s$) [43] | n/a | n/a | 1 | 1 |
| F_s | Stall force of myosin (pN) [44] | n/a | n/a | 3.85 | 3.85 |
| Crosslinkers | | | | | |
| l_{cl} | Rest Length (Filamin) (μm) [45] | n/a | 0.150 | n/a | 0.150 |
| k_{cl} | Stiffness ($pN/\mu m$) | n/a | 1, 10 | n/a | 1 |
| k_{cl}^{on} | Attachment rate at distance $r = 0$ (s^{-1}) | n/a | $10^6, 10^5$ | n/a | 3600 |
| k_{cl}^{off} | Unloaded head detachment rate (s^{-1}) | n/a | 0 | n/a | 0.2 |
| x_{cl} | characteristic bond length (μm) | n/a | 0.0004 | 0.0004 | 0.0004 |
| Environment | | | | | |
| dt | Dynamics timestep (s) | 10^{-4} | $10^{-6}, 10^{-5}$ | 2.5×10^{-4} | 2.5×10^{-4} |
| T_F | total simulated time (s) | 100 | 0.5 | 100 | 500 |
| X, Y | Length and width of assay (μm) | n/a | 75 | 50 | 75 |
| r_c | Mesh (actomyosin binding site) size (μm) | n/a | 0.2 | 0.2 | 0.2 |
| T | $k_B * \text{Temperature}$ ($pN\mu m$) | 0.004 | 0.004 | 0.004 | 0.004 |
| ν | Dynamic viscosity ($mg/(\mu ms)$) | 0.001 | 0.001 | 0.001 | 0.001 |
| γ | Strain (%) [46] | n/a | 0.001 | n/a | n/a |
| t_{relax} | Amount of time between sequential strains (s) | n/a | 0.001 | n/a | n/a |

- [11] Samantha Stam, Shiladitya Banerjee, Simon Freedman, Kimberly Weirich, Aaron R Dinner, and Margaret L Gardel. Filament rigidity and connectivity tune the deformation modes of active cytoskeletal networks. *in preparation*.
- [12] Stanislav Burov, S.M. Ali Tabei, Toan Huynh, Michael P. Murrell, Louis H. Philipson, Stuart A. Rice, Margaret L. Gardel, Norbert F. Scherer, and Aaron R. Dinner. Distribution of directional change as a signature of complex dynamics. *Proceedings of the National Academy of Sciences*, 110(49):19689–19694, 2013.
- [13] M.L. Gardel, J.H. Shin, F.C. MacKintosh, L. Mahadevan, P. Matsudaira, and D.A. Weitz. Elastic behavior of cross-linked and bundled actin networks. *Science*, 304(5675):1301–1305, 2004.
- [14] Minakshi Guha, Mian Zhou, and Yu-li Wang. Cortical actin turnover during cytokinesis requires myosin ii. *Current biology*, 15(8):732–736, 2005.
- [15] Cyrus A Wilson, Mark A Tsuchida, Greg M Allen, Erin L Barnhart, Kathryn T Applegate, Patricia T Yam, Lin Ji, Kinneret Keren, Gaudenz Danuser, and Julie A Theriot. Myosin ii contributes to cell-scale actin network treadmilling through network disassembly. *Nature*, 465(7296):373–377, 2010.
- [16] F.C. MacKintosh, J. Käs, and P.A. Janmey. Elasticity of semiflexible biopolymer networks. *Physical Review Letters*, 75(24):4425, 1995.
- [17] D. A. Head, A. J. Levine, and F. C. MacKintosh. Distinct regimes of elastic response and deformation modes of cross-linked cytoskeletal and semiflexible polymer networks. *Phys. Rev. E*, 68:061907, Dec 2003.
- [18] Jan Wilhelm and Erwin Frey. Elasticity of stiff polymer networks. *Physical Review Letters*, 91(10):108103, 2003.
- [19] Taeyoon Kim, Wonmuk Hwang, Hyungsuk Lee, and Roger D. Kamm. Computational analysis of viscoelastic properties of crosslinked actin networks. 2009.
- [20] Francois Nedelec and Dietrich Foethke. Collective langevin dynamics of flexible cytoskeletal fibers. *New Journal of Physics*, 9(11):427, 2007.
- [21] Thorsten Erdmann and Ulrich S. Schwarz. Stochastic force generation by small ensembles of myosin ii motors. *Physical Review Letters*, 108(18):188101, 2012.
- [22] Samantha Stam, Jon Alberts, Margaret L. Gardel, and Edwin Munro. Isoforms confer characteristic force generation and mechanosensation by myosin ii filaments. *Biophysical journal*, 108(8):1997–2006, 2015.
- [23] Daniel Gordon, Anne Bernheim-Groswasser, Chen Keasar, and Oded Farago. Hierarchical self-organization of cytoskeletal active networks. *Physical Biology*, 9(2):026005, 2012.
- [24] Taeyoon Kim. Determinants of contractile forces generated in disorganized actomyosin bundles. *Biomechanics and modeling in mechanobiology*, 14(2):345–355, 2014.

- [25] G.H. Koenderink, M. Atakhorrami, F.C. MacKintosh, and C.F. Schmidt. High-frequency stress relaxation in semiflexible polymer solutions and networks. *Physical Review Letters*, 96(13):138307, 2006.
- [26] KE Kasza, GH Koenderink, YC Lin, CP Broedersz, W Messner, F Nakamura, TP Stossel, FC MacKintosh, and DA Weitz. Nonlinear elasticity of stiff biopolymers connected by flexible linkers. *Physical Review E*, 79(4):041928, 2009.
- [27] Yi-Chia Lin, Norman Y. Yao, Chase P. Broedersz, Harald Herrmann, Fred C. MacKintosh, and David A. Weitz. Origins of elasticity in intermediate filament networks. *Physical Review Letters*, 104(5):058101, 2010.
- [28] William A Comrie, Shuixing Li, Sarah Boyle, and Janis K Burkhardt. The dendritic cell cytoskeleton promotes t cell adhesion and activation by constraining icam-1 mobility. *The Journal of cell biology*, 208(4):457–473, 2015.
- [29] Taeyoon Kim, W Hwang, and RD Kamm. Computational analysis of a cross-linked actin-like network. *Experimental Mechanics*, 49(1):91–104, 2009.
- [30] Monika Scholz, Stanislav Burov, Kimberly L Weirich, Björn J Scholz, SM Ali Tabei, Margaret L Gardel, and Aaron R Dinner. Cycling state that can lead to glassy dynamics in intracellular transport. *Physical Review X*, 6(1):011037, 2016.
- [31] M. Murrell. personal communication.
- [32] Tamara S Fraley, Clifford B Pereira, Thuan C Tran, CoreyAyne Singleton, and Jeffrey A Greenwood. Phosphoinositide binding regulates α -actinin dynamics mechanism for modulating cytoskeletal remodeling. *Journal of Biological Chemistry*, 280(15):15479–15482, 2005.
- [33] Michael Rubinstein and Ralph H. Colby. *Polymer Physics*. OUP Oxford, 2003.
- [34] R. Everaers, F. Jülicher, A. Ajdari, and A.C. Maggs. Dynamic fluctuations of semiflexible filaments. *Physical Review Letters*, 82(18):3717, 1999.
- [35] George I. Bell. Models for the specific adhesion of cells to cells. *Science*, 200(4342):618–627, 1978.
- [36] Jeffrey T. Finer, Robert M. Simmons, James A. Spudich, et al. Single myosin molecule mechanics: piconewton forces and nanometre steps. *Nature*, 368(6467):113–119, 1994.
- [37] Sam Walcott, David M. Warshaw, and Edward P. Debold. Mechanical coupling between myosin molecules causes differences between ensemble and single-molecule measurements. *Biophysical journal*, 103(3):501–510, 2012.
- [38] Benedict Leimkuhler and Charles Matthews. Rational construction of stochastic numerical methods for molecular sampling. *Applied Mathematics Research eXpress*, page abs010, 2012.
- [39] Benedict Leimkuhler and Charles Matthews. Robust and efficient configurational molecular sampling via langevin dynamics. *The Journal of Chemical Physics*, 138(17):174102, 2013.

- [40] Theo Odijk. The statistics and dynamics of confined or entangled stiff polymers. *Macromolecules*, 16(8):1340–1344, 1983.
- [41] A. Ott, M. Magnasco, A. Simon, and A. Libchaber. Measurement of the persistence length of polymerized actin using fluorescence microscopy. *Physical Review E*, 48(3):R1642, 1993.
- [42] Richard Niederman and Thomas D. Pollard. Human platelet myosin. ii. in vitro assembly and structure of myosin filaments. *The Journal of Cell Biology*, 67(1):72–92, 1975.
- [43] Stephen J. Kron and James A. Spudich. Fluorescent actin filaments move on myosin fixed to a glass surface. *Proceedings of the National Academy of Sciences*, 83(17):6272–6276, 1986.
- [44] Claudia Veigel, Justin E. Molloy, Stephan Schmitz, and John Kendrick-Jones. Load-dependent kinetics of force production by smooth muscle myosin measured with optical tweezers. *Nature Cell Biology*, 5(11):980–986, 2003.
- [45] Jorge M. Ferrer, Hyungsuk Lee, Jiong Chen, Benjamin Pelz, Fumihiko Nakamura, Roger D. Kamm, and Matthew J. Lang. Measuring molecular rupture forces between single actin filaments and actin-binding proteins. *Proceedings of the National Academy of Sciences*, 105(27):9221–9226, 2008.
- [46] Jonathan Stricker, Tobias Falzone, and Margaret L. Gardel. Mechanics of the f-actin cytoskeleton. *Journal of biomechanics*, 43(1):9–14, 2010.
- [47] H. Kojima, A. Ishijima, and T. Yanagida. Direct measurement of stiffness of single actin filaments with and without tropomyosin by in vitro nanomanipulation. *Proceedings of the National Academy of Sciences*, 91(26):12962–12966, 1994.
- [48] Hideo Higuchi, Toshio Yanagida, and Yale E. Goldman. Compliance of thin filaments in skinned fibers of rabbit skeletal muscle. *Biophysical Journal*, 69(3):1000, 1995.
- [49] C. Frontali, E. Dore, A. Ferrauto, E. Gratton, A. Bettini, M.R. Pozzan, and E. Valdevit. An absolute method for the determination of the persistence length of native dna from electron micrographs. *Biopolymers*, 18(6):1353–1373, 1979.

6 Supplement

6.1 Results

- 6.1.1 Bundling dependence on crosslinker density**
- 6.1.2 Polarity sorting dependence on motor detachment rate**
- 6.1.3 Contractile dependence on motor detachment rate**

6.2 Methods

6.2.1 Actin Filament Parameter Value Choices

For a confined semiflexible filament, it has been show that for a polymer of a given persistence length L_p , the shortest length that should be considered as unbending (l_a) is given by $l_a \approx$

$A^{2/3}L_p^{1/3}$ where A is a length scale associated with the confinement of the filament [40]. In these simulations, filaments were confined by nearby motors and crosslinkers. Since the smallest motor or crosslinker density used was $\rho_m = 0.1\mu m^{-2}$, $A \geq 1/\sqrt{0.1\mu m^{-2}} \Rightarrow l_a \geq 5\mu m$. In general, we used $l_a = 1\mu m$. The bending force constant is derived from the persistence length L_p such that $\kappa_B = L_p k_B T$ where k_B is Boltzmann's constant and T is the temperature .

Experimentally, the stretching force constant has been measured to be in the approximate range $k_a = 40 - 70 pN/nm$ [47, 48]; however, simulating a network of filaments with this large of a stiffness is computationally inefficient since the maximum timestep of a simulation is inversely proportional to the largest stiffness in the simulation. Therefore, we chose $\frac{\kappa_B}{l_a} \ll k_a$, so that the filaments were still much easier to bend than to stretch, enabling us to run simulations of experimentally relevant dimension. We show that our simple filament model exhibits expected behavior for a semiflexible filament in the next section and we have further verified that k_a did not effect the persistence length of the filament.

6.2.2 Explanation of Figure 7

Since actin bending is instrumental for actomyosin contraction, and simulating precise bending moduli is non-trivial, we tested our filaments by measuring spatial and temporal fluctuations and comparing with theoretical predictions. In a two dimensional WLC, a bending of two adjacent segments is expected to result in a local change in free energy of $\frac{\kappa_B}{2l_a\theta_i^2}$, and it is predicted that [49]

$$\langle \theta^2(l) \rangle = \frac{l}{L_p} \quad (10)$$

$$\langle \cos(\theta(l)) \rangle = \exp(-l/2L_p) \quad (11)$$

where $\theta(l) = \theta_j - \theta_i$ where $1 < i < j \leq N$, $l = l_a(j-i)$ and L_p is the persistence length. To test our model against these equations, we simulate 100 filaments of $L = 200\mu m$ and $\kappa_B = 0.08 pN\mu m^2$ at $T = 300K$ for $T_f = 100s$ and measured the resulting filament configuration every 1s. We discard the first 10 seconds of each simulation to allow equilibration, and we used only the middle $150\mu m$ of the filament to calculate these correlation functions. We have also shown that the measured persistence length, obtained by performing a least squares fit to plots of $\log(\langle \cos(\theta(l)) \rangle)$ for various values of κ_B yields the expected result over 3 orders of magnitude.

An additional prediction for semiflexible filaments is the scaling of fluctuations with time. Fluctuations transverse to the filament orientation have been shown to increase as a function of time as $\langle dr_{\perp}^2 \rangle \propto t^{3/4}$ while longitudinal fluctuations have been shown to follow the power law $\langle dr_{\parallel}^2 \rangle \propto t^{7/8}$ [34]. To tests these predictions, we followed the procedure outlined in [34] and generated $N = 100$ initial filament configurations of a $20\mu m$ filament. For each configuration we ran $M = 100$ simulations of the filament fluctuating for 1s. At each time step we collected the $2N$ positions of the filament ends, $r_e(t)$. We then calculated the eigenvalues of the covariance matrix $cov(r_e(t) \cdot \hat{i}, r_e(t) \cdot \hat{j})$ where $i, j \in \{x, y\}$. The larger eigenvalue $\lambda_1(t)$ corresponds to the slower longitudinal fluctuations (i.e., $\lambda_1(t) \propto t^{7/8}$) while the smaller eigenvalue corresponded to the faster perpendicular fluctuations ($\lambda_2(t) \propto t^{3/4}$). We show in Figure 7B that our simulation exhibits scaling of these eigenvalues in good agreement with the prediction of Ref. [34].

6.3 Dynamics

The Langevin equations of motion for a spherical bead of mass m and radius R at position $r(t)$ at time t can be written,

$$m\ddot{r}(t) = F(t) + B(t) - 4\pi R\nu\dot{r}(t) \quad (12)$$

where $F(t)$ is the force on the particle due to its interactions and $B(t)$ is Brownian forcing term, to simulate a temperature, ν is the dynamic viscosity of the bead's environment, and we have used the Einstein relation for the damping term. Since the fastest motion in this simulation is that of the myosin, and a $0.4\mu m$ myosin minifilament moving at a speed of $1\mu m/s$ in a liquid at least as viscous as water ($\nu_D = 10^6\mu m^2/s$ dynamic viscosity) has a very low Reynold's number ($Re \approx 4 * 10^{-7}$) we can treat the dynamics in the overdamped limit where the equation of motion is Equation (12) without the acceleration term, i.e. with $m = 0$. Furthermore, in the limit of small Δt , we may write $\dot{r}(t) \approx \frac{r(t+\Delta t) - r(t)}{\Delta t}$. These two approximations allow us to rewrite Equation (12) as Equation (8)

6.4 Neighbor list implementation

Because the probability of motor attachment decays as a Gaussian function of distance from the filament, it would be highly inefficient to attempt motor attachments with every filament in the simulation. Rather, we choose to test for connections only within a cutoff distance $r_c > 3R/2$ (where R is defined above as in Equation (4)). A grid of lattice size $2r_c$ is drawn in the $2D$ plane of the simulation, and the position of a filament is approximated as the points on the grid nearest to the beads of the filament. Thus, to determine if a motor will bind to a filament at time t , it is sufficient to only attempt attachment to filaments that are indexed at the four nearest grid points to a motor.

6.5 Algorithm Pseudocode

In pseudocode we can describe each timestep of the simulation as follows

```
For Each Bead on Each Filament:  
    Update force from filament stretching  
    Update force from filament bending  
    Update position via Equation (8)  
  
For Each Head on each Motor (cross-linker)  
    If head is unattached  
        try to attach  
        Add up forces (stretching)  
    Update position via Equation (8)  
    If head is attached  
        Update position via Equation (8)  
        Try to detach  
        If not detached  
            Step toward barbed end  
            Update attached actin with stretch force  
    Update neighbor lists
```